SID-MAGS: SPUTUM IMAGE DENOISING VIA MULTI-SCALE DEEP ANALYSIS MODEL AND GAUSSIAN STAR FILTER

Amala Shiny, A¹, Sivagami, B²

¹Research scholar, Department of Computer Applications, S. T. Hindu College, Nagercoil, Manonmaniam Sundaranar University, Tirunelveli, India.

²Head and Associate Professor, Department of Computer Science and Applications, S.T. Hindu College, Nagercoil, India

Abstract

Tuberculosis (TB) is a contagious bacterial infection caused by Mycobacterium tuberculosis, primarily affecting the lungs but can spread to other organs. TB remains one of the top 10 leading causes of death globally. Microscopic TB images of Ziehl Neelsen-stained sputum smears are frequently degraded by impulse, or salt-and-pepper, noise, obscuring the visual structure of mycobacterium. Effective denoising of these images is therefore crucial for accurate diagnosis. This study introduces a novel Sputum image Denoising using Multi-scale Deep Analysis model and Gaussian star filter (SID-MAGS) denoising method, which effectively suppresses up to 99% of salt-and-pepper noise. The proposed SID-MAGS method integrates two filters: the Gaussian star filter (GSF) and the novel Multi-Scale Deep Analysis (MSDA) Model. The MSDA model enhances denoising by decomposing images into multiple scales and stages, enabling deep searching for noise-free pixels that correlate with the current noisy pixel. This decomposition into five different scales allows comprehensive noise removal, outperforming traditional techniques. Experimental evaluations using online and real-time clinical databases demonstrate that the proposed method reduces time consumption by 27.99% for 60% noise levels and achieves a Peak Signal-to-Noise Ratio (PSNR) of 29.61 dB for 90% noise, compared to 27.273 dB for the next best method. These results underscore the method's efficacy in preserving mycobacterial structures and contrast, making it a valuable preprocessing tool for automated TB diagnosis applications.

Keywords: Tuberculosis, Sputum image, Image denoising, Gaussian star filter, Multi-scale deep analysis.

1. Introduction

resulting in more gradual development of disease when the research are summarized as: compared with other bacterial infections [3]. It is a small, rodotherwise, it can be fatal. For pulmonary TB, sputum samples noise. from suspected TB patients are stained using the ZN procedure. background of the sputum smear sample's other cells and decomposes images into five scales. organisms will remain blue [4,5]. Throughout the world, tuberculosis has a high death rate. However, survival chances noise but also preserves the anatomical structures and contrast significantly increase with early detection.

In image segmentation and detection systems, image applications. preprocessing is a crucial stage. There are numerous different contrast improvement, brightness modification, etc [6]. time for 60% noise. Numerous external elements in the environment and The rest of the work is prearranged as follows: Section 2 transmission systems generate different noises, such as Poisson, summarizes a number of current papers on the image denoising. Gaussian, Salt-and-Pepper and Speckle noise in medical Section 3 offers a thorough description of the proposed

images. An impulsive form of noise in images is salt and pepper Tuberculosis (TB) is a chronic infectious respiratory illness that noise which is also quoted as impulse noise [7]. Data poses a major threat to human health. The global TB mortality communication problems, faults in the analog-to-digital rate is over 1.3 million people. Furthermore, it is extremely converter, and memory cell failure commonly create this noise. dangerous because it is easily transmitted via air medium, when It appears as erratically spaced-out white and black pixels, the patients are coughing, sneezing or speaking [1,2]. As a which can dramatically lower an image's quality. As a result, result, the tuberculosis disease has become a major issue for the numerous restoration techniques, including Wavelet, Median Indian government. TB is caused by a bacterium called filter and Mean filter have been developed to remove the Mycobacterium and other mycobacterium, it is slow growing, impulse noise in medical images [8]. The main contributions of

- The paper introduces a Sputum image Denoising using shaped, strictly aerobic and acid-fast bacillus. Early and Multi-scale Deep Analysis model and Gaussian star filter (SIDaccurate detection of Mycobacterium TB (MTB) is vital; MAGS) approach to effectively remove the salt-and-pepper
- The MSDA model consists of multi-scale image The TB bacillus will turn red as a result of the technique, but the generation and deep searching-based noise removal that
 - The proposed SID-MAGS approach not only reduces of mycobacterium in TB images for automatic TB diagnosis
- The method was tested on both online and real-time image preprocessing methods, including noise reduction, clinical databases, showing a 27.99% reduction in processing

proposed approach are presented in Section 4. The conclusion and future scope are explained in Section 5.

2. LITERATURE SURVEY

In recent years, numerous image denoising techniques have been suggested by researchers. A summary of many current images by reducing noise. Unlike the MDBUTMF Filter, which studies on image denoising techniques is given in this section. In 2020 Lin., et al., [9] designed a two-stage denoising switching methods to dynamically adjust window sizes. This technique based on local similarity is proposed for images adaptive approach preserves more image details during noise affected by random-valued impulse noise. In the first stage, reduction, leading to significant improvements in PSNR for noise detection is performed by calculating the local similarity between the target pixel and its neighbours. In the second stage, an improved bilateral filter uses geometric distance and local similarity to filter the identified noise pixels with a weighted computational complexity. Channel attention-based networks average of surrounding intensities. Experiments demonstrate was computationally intensive and challenging to implement on that this method outperforms popular denoising techniques in hardware. Some methods for high-density noise reduction can effectively removing noise while preserving image details.

networks for image denoising, demonstrating that channel informative channels strongly associated with noise. The proposed locally adaptive channel attention, which adapts to the salt-and-pepper noise in sputum images of TB diseases. image content and noise, further improving denoising quality. Experimental results show that their globally tuned denoising 3. PROPOSED METHODOLOGY and enhancing image quality.

hardware resource sharing and distance-oriented classification, (MSDAM). it reduces multiplier usage by 48% compared to previous methods. Additionally, a quantization technique minimizes the size of lookup tables. Experimental results show that the proposed design is economical while maintaining clock rate, frame rate, and image quality.

In 2020, Varatharajan [12] introduced the Decision Based Unsymmetrical Trimmed Modified Winsorized Variants (DBUTMWV) for eliminating high-density salt-and-pepper noise in images and videos. The method identifies outliers (0 or 255) within a 3x3 neighbourhood. If a pixel is noisy, its four neighbours are examined: if all are noisy, the pixel is replaced by their mean; if not, it uses the median or midpoint of the nonnoisy pixels. Unaffected pixels remain unchanged.

In 2020, Huang., et al., [13] introduced a method for denoising images affected by salt-and-pepper noise. This approach optimizes sparse approximation to restore images tainted by high-density impulse noise. It starts with inverse-distance weighting-based prediction to estimate noise-affected pixels followed by enhancing noise-free results using a sparse approximation based on DCT and ant colony optimization. Tests on a benchmark image dataset demonstrate that this method surpasses existing techniques in removing image noise. In 2020 Senthil Selvi., et al., [14] devised a HFGOA approach, combining a hybrid filter, fuzzy logic structure, and genetic algorithm to restore images corrupted by impulse noise. Initially, the noisy image is de-noised using mean and median filters. The difference vector between the outputs of these filters is then computed and input into a fuzzy logic system. In the final step, a genetic optimization technique selects the optimal rule.

approach for denoising the sputum images. The fallouts of the Experimental results show that the HFGOA approach enhances image visual quality by increasing the PSNR value than the existing filters.

> In 2020 Sheela and Suganthi [15] designed an Adaptive Switching Modified Decision Based Unsymmetric Trimmed Median Filter (ASMDBUTMF) to enhance grayscale MRI uses fixed 3x3 window sizes, ASMDBUTMF employs adaptive severely contaminated images.

From these literature survey, despite advancements in denoising techniques struggle with real-time applications due to struggle with very high-density noise, and an adaptive approach In 2020 Lee., et al., [10] introduced channel attention-based face efficiency issue in handling extremely noisy images. To overcome these challenges, we introduced Sputum image attention enhances denoising by focusing the network on Denoising using Multi-scale Deep Analysis model and Gaussian star filter SID-MAGS approach to effectively remove

network outperforms current existing methods in both blind and In this section, a novel SID-MAGS approach is introduced for non-blind scenarios, significantly reducing computation time efficient denoising of sputum TB images. Figure 1 shows the overall diagram of the proposed SID-MAGS denoising method. In 2020 Lien., et al., [11] presented a cost-effective bilateral This method is constituted by two denoising filters namely filter hardware design for real-time image processing. Utilizing Gaussian star Filter (GSF) and Multi Scale Deep Analysis Model

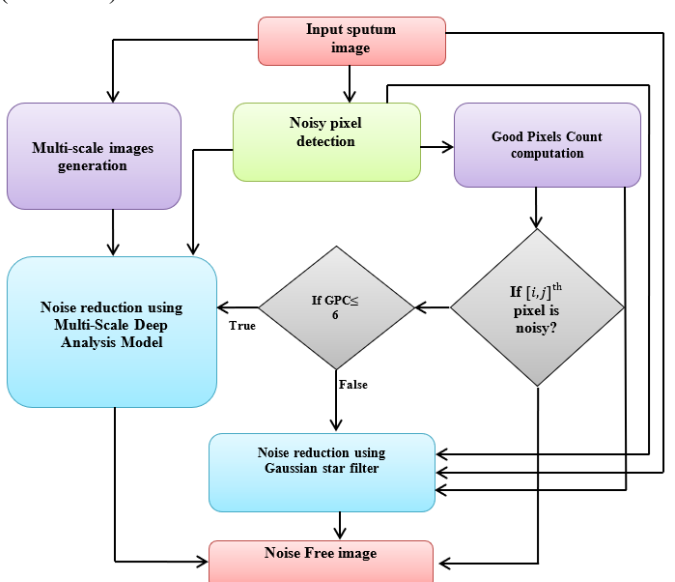


Figure.1: The overall workflow of the proposed SID-MAGS approach

3.1. Noisy pixel detection

Impulse noise type is one of the noises usually occurred in microscopic images. The salt noise is indicated by the intensity value of 255 while the pepper noise is indicated by the intensity value of 0. The input image of the size 512×512 is fed as input to this module. It should be a 24 bit Bitmap image and it

can be noted as
$$I_{IP}$$
. The noisy position of corrupted image is determined using Equation (1).
$$I_{NS}^{i,j,c} = \begin{cases} 0, & \text{if } I_{IP}^{i,j,c} = 0 \mid I_{IP}^{i,j,c} = 255 \\ 1, & \text{else} \end{cases}$$

$$i \in [0, H-1], & j \in [0, W-1], & c \in [0, C-1]$$
Where I_{NC} = Noisy status image $[H]$ - Image height (let it be 512) where I_{NC} = Noisy status image $[H]$ - Image height (let it be 512) and $[I_{NS}^{i,j} = I_{NS}^{i,j} = I_{N$

W - Image width (let it be 512) and C - Count of color channels In Equation (2), the absolute difference between red and green (let it be 3). In Equation (1), the pixels belong to the intensity value 0 or 255 are noted as noisy pixels and stored in $I_{NS}^{i,j,c}$ using the indicator value of 0. The non-noisy pixels are stored by the value of 1 in noisy status image.

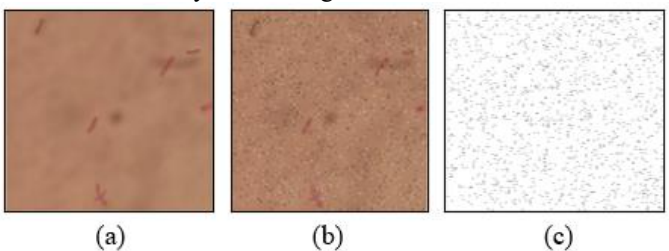


Figure.2: Representation of noise detection, (a) input MTB image, (b) noisy image, (c) noise status image.

Figure 2 depicts the noise detection process. Figure 2(a) shows the input sputum smear image. Herein, the pinkish bacilli are known as MTB bacilli which are exposed by microscope. Figure 2(b) shows the noisy MTB image which reveals the salt and pepper noise. Figure 2(c) illustrates the noisy status image that points out the noisy positions and non-noisy positions by using the binary values 0 and 1 respectively.

3.2. Good Pixels Count Computation

The term good pixel refers the probably unaffected pixels by noise in the surrounded window kernel. In this section, the good pixels of a 5 × 5 window kernel is determined and the count of them are computed. This computation is influenced by the pairs of 3 color channels such as red, green and blue. It involves six mathematical operations includes Deviation between pair of color channels, Average deviation computation, Absolute deviation computation, Average absolute deviation computation, A difference value computation and Good pixel computation.

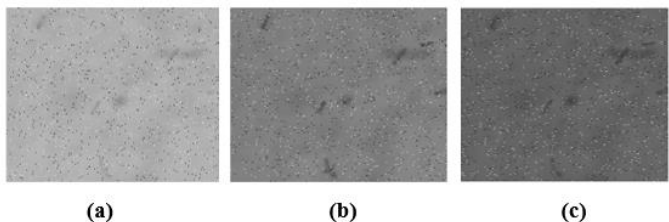


Figure.3: Representation of color components, (a) Red channel, (b) Green channel, (c) Blue channel.

The MTB color images are made up of red, green, and blue channel color components. They are illustrated in Figure 3 where the red channel is represented by Figure 3(a), the green channel is shown by the Figure 3(b), and the Figure 3(c)showcases the blue channel of the RGB color image. Herein, each color channel highlights its unique representation in brightness and contrast properties. The red channel image is channel image is presented by the term I_B . The deviation between the color pair are computed for each pixel using Equation (2), Equation (3) and Equation (4).

$$\Delta_{rq}^{i,j} = \left| I_R^{i,j} - I_G^{i,j} \right| \tag{2}$$

$$\Delta_{ab}^{i,j} = \left| I_G^{i,j} - I_B^{i,j} \right| \tag{3}$$

$$\Delta_{rb}^{i,j} = \left| I_R^{i,j} - I_R^{i,j} \right| \tag{4}$$

Where I_{NS} - Noisy status image, H - Image height (let it be 512), pair, Δ_{gb} - Deviation of GB pair and Δ_{rb} - Deviation of RB pair. channels is computed. In Equation (3), the absolute difference between the green and blue channels are calculated. The absolute difference between the red and blue channel is computed using Equation (4). The mean value of 'color channel deviation' shows the common deviation value between the color channel pairs. It can be computed using Equation (5).

$$\Delta_{rg}^{avg} = \frac{\sum_{l=0}^{H-1} \sum_{j=0}^{W-1} \Delta_{rg}^{l,j}}{\sum_{rg}^{H+1} \Delta_{rg}^{W-1}}$$
(5)

 $\Delta_{rg} = \frac{\Delta_{rg}}{H \times W}$ (5) Where Δ_{rg}^{avg} - Average deviation of red and green channels. In the similar manner, the average deviation of GB channels is computed and noted as Δ_{gb}^{avg} . In the similar fashion, the average deviation of red and blue channel is calculated and stored as Δ_{rh}^{avg} . Good pixels counting process is progressed by constructing a rule which is influenced by the difference values of color channels. It can be computed using Equation (6) and Equation (7).

$$\gamma^{i,j} = \sum_{p=-2}^{2} \sum_{q=-2}^{2} f(i+p,j+q) \tag{6}$$

$$f(x,y) = \begin{cases}
1, & \text{if } \beta_{rg}^{x,y} < \alpha_{rg}^{avg} & \text{\& } \beta_{gb}^{x,y} < \alpha_{gb}^{avg} & \text{\& } \beta_{rb}^{x,y} < \alpha_{rb}^{avg} \\
0, & \text{else}
\end{cases} \tag{7}$$

Where $i \in [2, H-3]$, $j \in [2, W-3]$; $\gamma^{i,j}$ - Good pixel count array for $[i,j]^{th}$ pixel and f(x,y) - General function to compute good pixels count. The frequency of good pixels in a 5×5 kernel related to $[i,j]^{th}$ pixel is computed using the six parameters such as β_{rg} , α_{rg}^{avg} , β_{gb} , α_{gb}^{avg} , β_{rb} and α_{rb}^{avg} . If the good pixel count for a specific noisy pixel is greater than 7, then the Gaussian Star Filter is applied; otherwise, MSDA model is applied.

3.3. Gaussian star filter

A Gaussian star filter is a variation of the Gaussian filter tailored for specific applications, such as sputum image denoising. The Gaussian filter is a widely-used filter in image processing, defined by the Gaussian function:

$$G(x,y) = \frac{1}{2\pi\sigma^2} e^{-\frac{x^2 + y^2}{2\sigma^2}}$$
(8)

Where x and y are the coordinates of the pixel. σ is the standard deviation of the Gaussian distribution, controlling the spread of the Gaussian kernel. The Gaussian star filter extends the concept of the Gaussian filter by applying a star-shaped mask, focusing on denoising while maintaining the geometric features of the sputum image. Compute the Gaussian kernel G(x, y) for the desired standard deviation σ . Define a star-shaped mask S that emphasizes certain directions (e.g., horizontal, vertical, and diagonal). Given an image I and a star-shaped mask SSS, the Gaussian star-filtered image *I* was represented as:

$$I'(x,y) = \sum_{i=k}^{k} \sum_{j=k}^{k} I(x+i, y+j) \times G(i,j) \times S(i,j)$$
 (9)

Where I(x + i, y + j) is the intensity of the neighboring pixel, G(i,j) is the Gaussian kernel value, S(i,j) is the star mask marked by I_R , green channel is quoted by I_G and the blue value (0 or 1) that determines whether the Gaussian weight is applied at position (i, j)(i, j) and k is the kernel radius, typically determined by σ . The Gaussian star filter's combination of Gaussian smoothing and directional emphasis makes it a

enhancing sputum smear images affected by noise.

3.4. Multi-Scale Deep Analysis Model

MSDA model is the novel filter designed by this research to effectively remove the salt and pepper noise in sputum smear microscopic images. The MSDA model is suitable to denoise the huge range of impulsive noise environment in medical and other images. It can be applied to denoise the impulse noisy pixels that have less than seven surrounded good-pixels because

pixels that have less than seven surrounded good-pixels occased lesser count of good pixels refers the highly contaminated noisy pixel. $I_{256\times256}^{fix\left(\frac{j}{2}\right),fix\left(\frac{j}{2}\right),0,p\times b+q}=I_{IP}^{i+p,j+q,ch=0}$ The multi-scale image analysis means the processing of small dimensional of images which are decomposed by multiple scales with multi-stages to target the aim of the research. The multi-scale image analysis means the processing of small $I_{256\times256}^{fix\left(\frac{j}{2}\right),fix\left(\frac{j}{2}\right),1,p\times b+q}=I_{IP}^{i+p,j+q,ch=1}$ with multi-stages to target the aim of the research. The multi-scale image analysis means the processing of small $I_{256\times256}^{fix\left(\frac{j}{2}\right),fix\left(\frac{j}{2}\right),2,p\times b+q}=I_{IP}^{i+p,j+q,ch=1}$ scale image analysis decomposes the images into a unique $I_{256\times256}^{(2)}$ dimension based on a specific scale. In this research, five different scales are followed to make five stages of deep [0, b-1] For further scales, the same logic applies, adjusting searching for noise free pixels as shown in figure 4. It acts as a the block size b accordingly. The denoised output image that deep learning model to determine the scattered noise free pixels, which is impossible one for traditional denoising methods. This MSDA model provides a pioneered result than the trimmed switching window concept and the fuzzy concept. So, the positions of surrounding noise free pixels can be found from comparatively near-by positions. The blurring artifact is also reduced, besides that it also maintains the structural information of sputum smear microscopic images. Figure 3 depicts the block diagram of the proposed MSDA model.

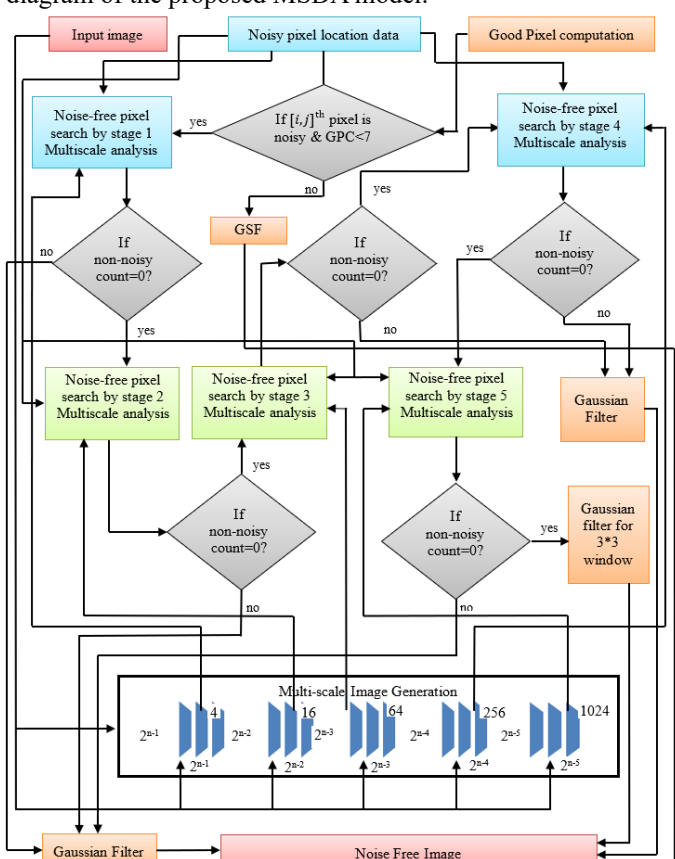


Figure.4: Block diagram of denoising using Multi-Scale **Deep Analysis Model**

3.5. Multi-scale image generation

In this section, a 512x512 image is used to generate multi-scale images by dividing it into progressively smaller sub-images.

valuable tool in medical image processing particularly for The process involves five scales: 256x256 (4 sub-images per channel), 128x128 (16 sub-images per channel), 64x64 (64 subimages per channel), 32x32 (256 sub-images per channel) and 16x16 (1024 sub-images per channel). Each colour channel (red, green, blue) is processed individually. For the red channel, sub-images are labelled as $I_{256\times256}^{i,j,ch=0,si}$, where i,j are row/column positions, ch is the colour channel, and si is the sub-image index. The generation of sub-images is illustrated with the

$$I_{256\times256}^{fix(\frac{1}{2}),fix(\frac{1}{2}),0,p\times b+q} = I_{IP}^{i+p,j+q,ch=0}$$
 (10)

$$I_{256\times256}^{fix(\frac{1}{2}),fix(\frac{J}{2}),1,p\times b+q} = I_{IP}^{i+p,j+q,ch=1}$$
 (11)

$$I_{256\times256}^{fix(\frac{1}{2}),fix(\frac{1}{2}),2,p\times b+q} = I_{IP}^{i+p,j+q,ch=2}$$
 (12)

Where $i \in [0,H-1], j \in [0,W-1], p \in [0,b-1], q \in$ contains the restored/enhanced noise free information. Even though the noise corruption is 97%, the basic structures of the filter is exposed by the proposed SID-MAGS approach.

4. RESULTS AND DISCUSSION

This section provides an assessment on the proposed denoising method namely SID-MAGS approach against existing denoising methods to prove the efficiency of the proposed method. This analysis includes 3 existing methods to have a better evaluation of the proposed method with the three existing denoising methods. In this research, the MSE analysis is used to inspect the performance range of the proposed denoising method against the three existing methods. The MSE computation is progressed using Equation (13).

$$MSE_{DNS} = \frac{1}{H \times W} \sum_{i=0}^{H-1} \sum_{j=0}^{W-1} \left(I_{ORIG}^{i,j} - I_{NF}^{i,j} \right)^2$$
 (13) where MSE_{DNS} - MSE for denoising process, I_{ORIG} - Original

tuberculosis MTB image, I_{NF} - Noise Free tuberculosis MTB image. In Equation (13), the two parameters like I_{ORIG} and I_{NF} involve to compute the error value in the similarity between the original image and the restored image. The best denoising method always scores lower MSE values.

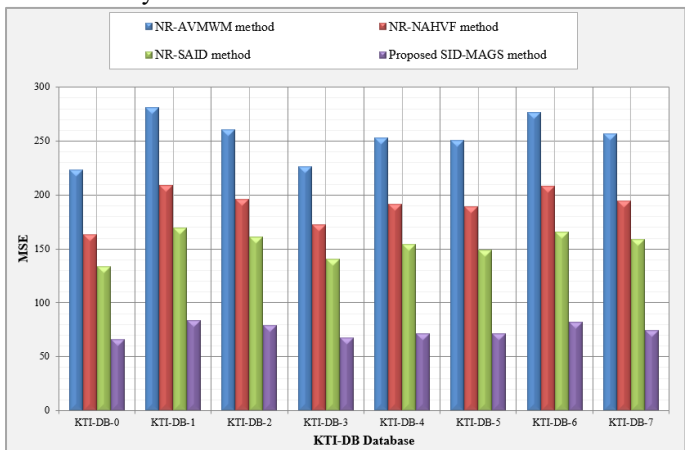


Figure.5: MSE analysis chart on KTI-DB database

Figure 5 for the four approaches such as NR-AVMWM, NR-NAHVF, NR-SAID and the proposed SID-MAGS approach. According to the hypothesis, the optimal approach is the one with the lowest MSE value. The proposed SID-MAGS approach is the lowest MSE provider in this investigation. The MSE of the SID-MAGS approach has the lowest value of 65.476 which input TB image (I_{ITB}) , noisy TB image (I_{NTB}) and noise free corresponds to KTI-DB-0 image.

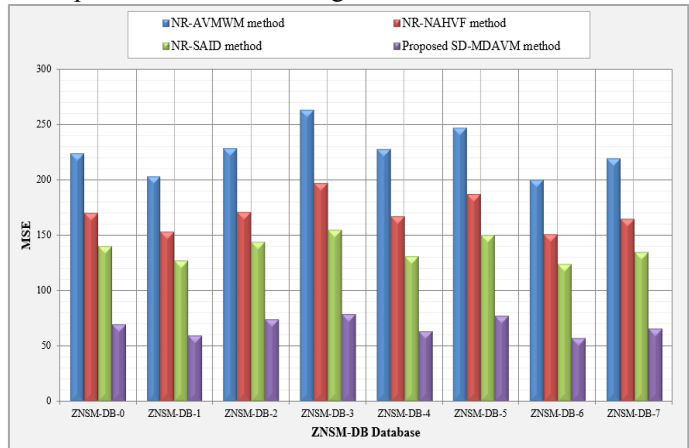


Figure.6: MSE analysis chart for ZNSM-DB database

Figure 6, the MSE statistic of denoising-performance is investigated. For 90 percent noise corruption on MTB TB images, the MSE study uses four techniques: NR-AVMWM, NR-NAHVF, NR-SAID and the proposed SID-MAGS approach. Among the four filters utilized in this investigation, the NR-AVMWM filter has the highest MSE. As a result, the NR-AVMWM denoising filter yields the worst outcomes. The best denoising technique for 90% noise contamination is the proposed SID-MAGS approach, which has the least MSE.

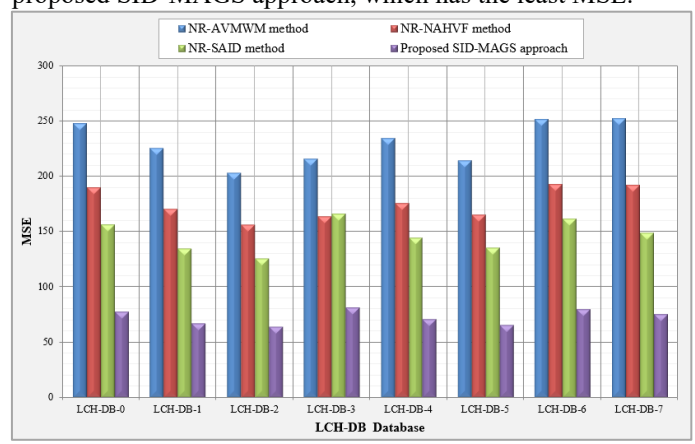


Figure.7: MSE analysis chart on LCH-DB database

Figure 7, the MSE statistic of denoising performance is examined for 90 percent noise corruption on MTB TB images. As a result, it yields the worst outcomes.

calculates the image quality with referred to original image, higher IEF notifies the best denoising algorithm and vice versa. preprocessing tool for automated TB diagnosis applications. The IEF computation is engaged with the parameters, such as

TB image (I_{NFTB}), and it can be computed following equations.

$$E_{1} = \sum_{i=0}^{H-1} \sum_{j=0}^{W-1} (I_{NTB}^{i,j} - I_{ITB}^{i,j})^{2}$$

$$E_{2} = \sum_{i=0}^{H-1} \sum_{j=0}^{W-1} (I_{NFTB}^{i,j} - I_{ITB}^{i,j})^{2}$$
(14)

$$E_2 = \sum_{i=0}^{H-1} \sum_{j=0}^{W-1} \left(I_{NFTB}^{i,j} - I_{ITB}^{i,j} \right)^2$$
 (15)

$$IEF = \frac{E_1}{E_2} \tag{16}$$

Where E_1 - Square error of noisy TB image and input TB image, E_2 - Square error of noise free TB image and input TB image and IEF - Image enhancement factor for denoising the TB image.

Table.1: Average IEF analysis on three different databases

Database	Average IEF analysis			
name	NR- AVMWM method	NR- NAHVF method	NR- SAID method	Proposed SID- MAGS approach
KTI-DB	133.588	144.883	162.504	306.911
ZNSM- DB	146.319	155.180	170.635	322.532
LCH-DB	138.766	147.279	167.335	311.480

The average image enhancement factors of three TB databases are displayed in Table 1. For this analytical assignment, test databases such as KTI-DB, ZNSM-DB and LCH-DB are employed. This study is carried out using the 90 percent noisy corruption. This IEF measure is analyzed using different methods, including NR-AVMWM, NR-NAHVF, NR-SAID and the Proposed SID-MAGS approach. The KTI-DB database was reported to yield the second-highest average IEF value, indicating that it is the second-best database for image enhancement factor. The least IEF average is found in the LCH-DB database. Out of the three databases examined in this study, the LCH-DB database has the least image enhancement factor. The Proposed SID-MAGS approach provides higher valued IEF results compared to existing methods for the entire three databases which proves the denoising-efficiency of the proposed SID-MAGS approach.

5. CONCLUSION

This paper introduces a novel SID-MAGS denoising method, which effectively suppresses up to 99% of salt-and-pepper noise. The proposed SID-MAGS method integrates two filters: the GSF and the MSDA Model. The MSDA model enhances The MSE analysis uses four techniques: NR-AVMWM, NR- denoising by decomposing images into multiple scales and NAHVF, NR-SAID and the proposed SD-MDAVM filter. In stages, enabling deep searching for noise-free pixels that comparison to the other three filters already in use, the proposed correlate with the current noisy pixel. This decomposition into SD-MDAVM filter has the lowest MSE on the LCH-DB that five different scales allows comprehensive noise removal, makes it the best denoising approach. The NR-SAID filter is the outperforming traditional techniques. Experimental evaluations second-best method for denoising, according to this research. using online and real-time clinical databases demonstrate that Highest MSE value 251.81 is found in the NR-AVMWM filter. the proposed method reduces time consumption by 27.99% for 60% noise levels and achieves a PSNR of 29.61 dB for 90% The quality of image enhancement is analyzed based on the noise, compared to 27.273 dB for the next best method. metric namely Image Enhancement Factor. The IEF measure Consequently, the proposed SID-MAGS model is regarded as the optimal denoising technique compared to previous iterations. which can be used as a tool to compare the enhancement. These results underscore the method's efficacy in preserving efficiency of the proposed and existing algorithms. Generally, mycobacterial structures and contrast, making it a valuable

References

- 1. P. Saraswat and M. Singh Solanki, "Phishing Detection in E-mails using Machine Learning," 2nd International conference on technological advancements in computational sciences (ICTACS), Tashkent, Uzbekistan, pp. 420-424, 2022.
- 2. T. G. Rambabu and K.V.K. Kishore, 'Medical image denoising using KPCA with local pixel grouping', International conference on computer communication and informatics (ICCCI), pp. 1-5, 2022.
- 3. Z. HosseinKhani, M. Hajabdollahi, N. Karimi, R. Soroushmehr, S. Shirani, K. Najarian and S. Samavi, 'Adaptive real-time removal of impulse noise in medical images', Springer, Journal of medical systems, vol. 42, issue 11, pp. 1-9, (2018).
- 4. B. Fu, X. Zhao, C. Song, X. Li and X. Wang, 'A salt and pepper noise image de-noising method based on the generative classification', Springer, Multimedia tools and applications, vol. 78, issue 9, pp. 12043-12053, 2019.
- 5. J. Chen, Y. Zhan and H. Cao, 'Adaptive sequentially weighted median filter for image highly corrupted by impulse noise', IEEE Access, vol. 7, pp. 158545-158556, 2019.
- 6. M. Tian and K. Song, 'Boosting magnetic resonance image de-noising with generative adversarial networks', IEEE Access, vol. 9, pp. 62266-62275, 2021.
- 7. S. Rai, J.S.Bhatt and S.K. Patra, 'Augmented noise learning framework for enhancing medical image de-noising', IEEE Access, vol. 9, pp. 117153-117168, 2021.
- 8. Y. T. S. Pengand S. W. Huang, 'Image impulse noise removal using cascaded filtering based on overlapped adaptive Gaussian', vol. 2, pp. 382-392, 2021.

- 9. Lin, C., Li, Y., Feng, S. and Huang, M., 2020. A two-stage algorithm for the detection and removal of random-valued impulse noise based on local similarity. IEEE Access, 8, pp.222001-222012.
- 10. Lee, H. and Cho, S., 2020. Locally adaptive channel attention-based network for denoising images. IEEE Access, 8, pp.34686-34695.
- 11. Lien, C.Y., Tang, C.H., Chen, P.Y., Kuo, Y.T. and Deng, Y.L., 2020. A low-cost VLSI architecture of the bilateral filter for real-time image denoising. IEEE Access, 8, pp.64278-64283.
- 12. Varatharajan, R., 2020. A decision based unsymmetrical trimmed modified winsorized variants for the removal of high-density salt and pepper noise in images and videos. Computer communications, 154, pp.433-441.
- 13. Huang, S.C., Peng, Y.T., Chang, C.H., Cheng, K.H., Huang, S.W. and Chen, B.H., 2020. Restoration of images with high-density impulsive noise based on sparse approximation and ant-colony optimization. IEEE Access, 8, pp.99180-99189. 14. Senthil Selvi, A., Kumar, K.P.M., Dhanasekeran, S., Maheswari, P.U., Ramesh, S. and Pandi, S.S., 2020. De-noising of images from salt and pepper noise using hybrid filter, fuzzy logic noise detector and genetic optimization algorithm (HFGOA). Multimedia Tools and Applications, 79, pp.4115-4131.
- 15. Sheela, C.J.J. and Suganthi, G., 2020. An efficient denoising of impulse noise from MRI using adaptive switching modified decision based unsymmetric trimmed median filter. Biomedical Signal Processing and Control, 55, p.101657.